Proceedings World Geothermal Congress 2020+1
Reykjavik, Iceland, April - October 2021

Structural and Paleomagnetic Analysis of Geothermal Drill Core, Akutan Alaska

Molly Johnson[1], Pete Stelling[2]

[1,2] Western Washington University, Environmental Studies Building 240, 516 High St, Bellingham, WA 98225

Email: [1] johns877@wwu.edu, [2] stellip@wwu.edu

Keywords: Paleomagnetism, core reorientation, geothermal, structural geology

ABSTRACT

Hot Springs Bay Valley (HSBV) geothermal resource area on Akutan Island, Alaska, has increased fluid output and temperature by almost a magnitude, between 1981 and 2012 (Bergfeld et al., 2014). These increases have been attributed to increased permeability along NW-SE trending faults that may have been activated during a seismic swarm in 1996. In 2010 two unoriented drill cores were collected in Hot Springs Bay geothermal resource area. In this study we reorient sections from one the highly fractured core with paleomagnetics to test this model of geothermal reservoir evolution at Akutan. The core is composed of interlayered island arc volcanics and shallow marine mudstones. Paleomagnetic samples were collected from the volcanics. Continuous sections of the core were reoriented using the declination of the remanent magnetization (RM) as an indication of geographic north. Structure from motion software was used to create digital reconstructions of the core from photographs. The resulting models were then flattened with a cylindrical projection into a 2D depiction of the outside of the core. The orientation of veins and the relationship between vein sets were measured from these projections, while the rake of slicken line and mineralogy were determined in hand sample. Fracture sets were defined by mineralogy and The Multiple Inverse Method (MIM) was employed to calculate the stress regime that produced each fracture set. Results show that WNW-ESE trending calcite filled veins are the result periodic extension possibly caused by inflation of the volcano due to dike emplacement and represent recharge of the reservoir. NNW trending chlorite filled veins are the result of normal overburden pressure and likely represent the northward migration of heated fluids to the reservoir. Cross cutting relations indicate that NE and SW dipping, NW-SE trending structures are conjugate and have ruptured repeatedly. Therefore, events like the 1996 seismic swarm, which produced NW trending ground cracks have likely acted to maintain permeability throughout the lifetime of the geothermal system at Akutan.

1. INTRODUCTION

The City of Akutan and adjacent Trident Seafoods processing plant on Akutan Island (Figure 1B) would greatly benefit from a local source of clean energy. The City of Akutan and Trident Seafood's current energy needs are being met by burning 4.3 million gallons of imported diesel fuel annually (Kolker et al., 2011). In 2018 residential electricity rates in Akutan were 0.3117 $/kWh; 162% greater than the national average. The need here could be met by establishing a geothermal power plant in Hot Springs Bay Valley (HSBV) geothermal resource area, which would add valuable infrastructure to the island, help the community become more energy independent, and diversify the job market.

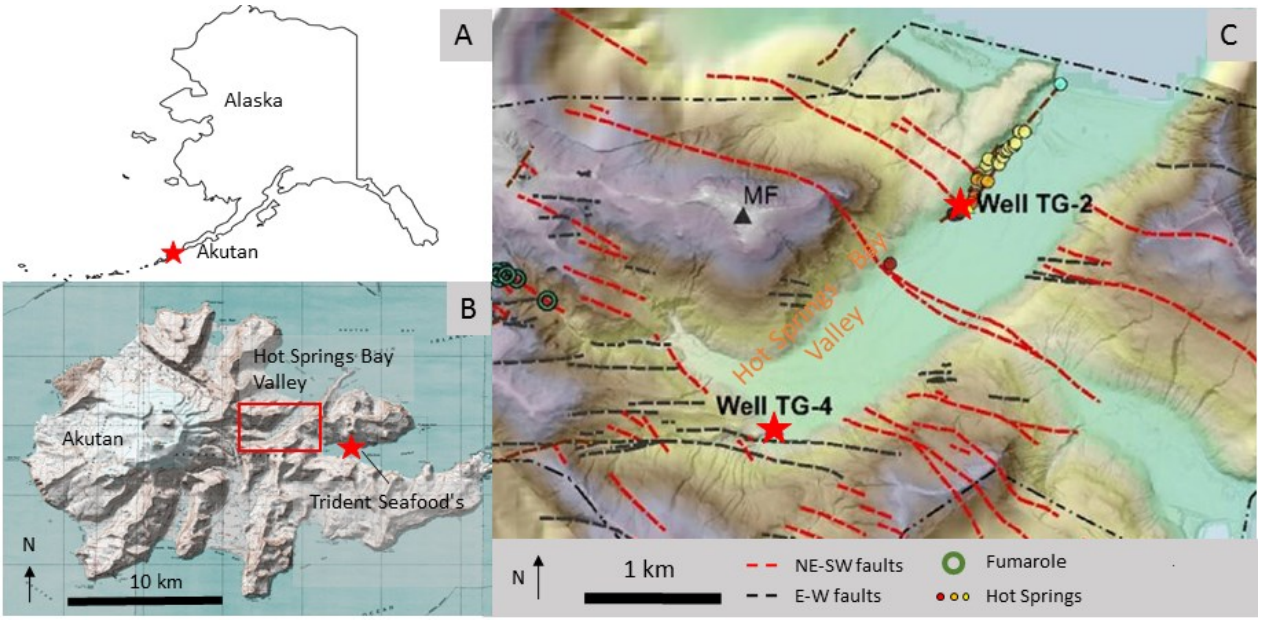

Figure 1: Map of A) Akutan in relation to Alaska denoted by the red star; B) the location of hot springs bay valley (HSBV), on Akutan Island (red box) and Trident Seafoods processing plant (red star); C) the location of well TG-4 and structural and geothermal features within HSBV. MF = Mt. Formidable. Modified from Stelling et al. 2015.

The Aleutian Island chain, and Akutan Island in particular (Figure 1A), has high potential for geothermal power production (Motyka et al., 1993; Kolker et al., 2012; Stelling et al., 2015). Previous geochemical studies (Bergfeld et al., 2014; Stelling et al., 2015) and down whole measurements of two slim wells (Kolker et al., 2011) have confirmed enough reservoir heat to produce 2-3 MWe from the resource (Stelling et al., 2015). Furthermore, Bergfeld et al., (2014) noted a 134% increase in discharge of the thermal creek and increased temperatures resulting in a 29MW thermal output for the hot springs, which is about a magnitude greater than previous studies (Motyka et al., 1988). These increases reflect both an increase in heat and an increase in permeability of the system between the early 1980's and 2012. Bergfeld et al., (2014) postulated that rupture of the NW-SE striking fault during the seismic swarm in 1996 could explain the increased permeability and notes the longevity of the increased heat output, if their hypothesis is indeed correct. The primary goal of this project is to determine the orientation of permeable fractures in the subsurface of the HSBV geothermal resource, and therefore test Bergfeld's hypothesis.

Both wells were recovered entirely as unoriented core, with variable degrees of fracturing. Well TG-2 is 254 m (833 ft.) deep, located on the northern side of the lower valley close to the eastern extent of the hot springs (Figure1C). Approximately 90% of the TG-2 core was recovered. Well TG-4 is 457.2 m (1500 ft.) deep and located along the southwestern valley wall at the confluence of the upper and lower valleys (Kolker et al., 2011), with core recovery of ~98% (Figure 1C). Reorientation of segments from TG-4 was done using the declination of RM in the core as an indicator of geographic north. Using RM is an inexpensive and proven technique for orienting already-drilled core (Fuller, 1969) and has been used widely in such varied studies as petroleum exploration (Allerton et al., 1995; Hailwood and Ding, 1995), by the Ocean Drilling Program to study the structure of subduction wedges (Hill et al., 1993), and to establish Magnetostratigraphic sections for the late-Triassic to early Jurassic (Kent et al., 1995). Yet there are several challenges employing this method at Akutan. The high latitude of Akutan results in a very steep inclination of the magnetic signal (72o in the modern field), and therefore the declination signal has a high degree on intrinsic error. Furthermore, the magnetic signal could have been overprinted by the actual drilling of the core (Hailwood and Ding, 1995). Because of these sources of error, we refer only generally to the direction of reoriented structures.

2. GEOLOGIC CONTEXT

Akutan Island is one of the easternmost Aleutian Islands, which is part of the volcanic arc formed from the northwestward subduction of the Pacific plate under the North American plate. The active volcano dominates the western half of the island. The eastern half of the island is composed of glacially scoured remnants of ancient volcanic activity. Romick et al., (1990) separated the rock units on Akutan into three broad categories. The oldest rocks on the island are the hot springs volcanics (HSV), overlain by the ancestral Akutan volcanics (AKV), and the modern Akutan volcanics (MOD) with the most recent lava flows in the north of the island. The AKV and MOD are separated by an angular unconformity (Romick et al., 1990). The AKV are cut by dikes of MOD which mostly parallel the ridges that extend out from Akutan volcano (Byers and Barth, 1953). Akutan has been the most active volcano in the region for decades (Finch, 1935; Miller et al., 1998). Historical records show that major activity on the volcano occurs approximately every 20 years (Byers and Barth, 1953), the most recent of which was a seismic swarm in 1996, which has been attributed to the emplacement of a shallow dike (Lu et al., 2005). Surface mapping shows three orientations of structural features on Akutan Island (Richter et al., 1998; Stelling et al., 2015). These are fault scarps, fractures, dikes and lineaments that are oriented WNW-ESE, NE-SW, and E-W (Figure 1C). There are two geothermal systems on Akutan (Motyka et al., 1993), one in the summit crater and one on the flank of the volcano in HSBV.

The seismic swarm of 1996 consisted of >3000 earthquakes (Mmax=5.1) that reactivated WNW-ESE striking faults south of HSBV and across the island (Lu et al., 2005). The change in ground surface morphology before and after the seismic activity is consistent with the emplacement of a dike with its shallowest depth at 0.4 km beneath the northwest flank of Akutan volcano oriented parallel to the WNW striking ground cracks (Lu et al., 2005). The documented subsidence on the south-east flank could be explained by depressurization of the hydrothermal field facilitated by movement along normal faults. Subsidence of the northwest flank in 1996-1997 by about 20mm is most likely due to the cooling and degassing of the intrusion (Lu et al., 2005).

HSBV is a glacially carved valley on the northeastern side of island. The upper valley is oriented NW-SE and the lower valley is oriented NE-SW. The two valleys meet in the southwest, forming an approximately 90^{o} bend (Figure 1C) suggesting that the glacier's path may have been structurally controlled. A prominent NW-SE striking normal fault cuts through HSBV and has a down-to-the-south slip direction (Richter et al. 1998). Most faults mapped in HSBV have dips to the south and show a down-to-the-south dip slip or oblique slip motion with dip angles between 50o and near vertical, however nearly a third of the faults mapped throughout the island do not have dip direction constrained. Fracture traces also dip between 50o and near vertical, but the dip direction is bimodal to the north and south (Stelling et al., 2015).

The HSBV hydrothermal system hosts a fumarole field at the head of the upper valley and a string of hot springs extending ~1 mile along the northern wall of the lower valley (Finch, 1935; Motyka et al., 1993; Symonds et al., 2003; Kolker et al., 2012; Bergfeld et al., 2014; Stelling et al., 2015). The fumaroles and the hot springs are likely connected and stem from the same deep reservoir. The current conceptual model by (Stelling et al., 2015) is based on gas geochemistry, silica and cation geothermometry, geophysics and down-hole temperature measurements. According to this model there is a high temperature upflow under the flank fumaroles that bifurcates into a lower temperature outflow daylighting at the hot springs. Kolker et al. (2012) proposed two different flow paths for the outflow, one following HSBV to the south, and the other curving north under Mt. Formidable just north of HSBV (Figure 1C). A geochemical study of the hot springs (Bergfeld et al., 2014) reported a heat output of ~29MW, which is about an order of magnitude higher than studies done in the 1980's (Motyka et al., 1993). Additionally, Bergfeld et al. (2014) reported a 20-25 percent increase in the flow of thermal streams, a ten degree increase in temperature of thermal springs as well as substantial increases in most dissolved solids which combined indicate an increase in hydrothermal activity. Bergfeld et al. (2014) suggest this increase in heat and discharge is the result of increased fracture density and dilation along the WNW-ESE oriented normal fault between the hot springs and the fumaroles that was re-activated during the 1996 seismic swarm.

The TG-2 well was drilled next to the hot springs to intercept the outflow. While TG-4 was drilled at the confluence of the upper and lower valleys where the three major orientations of faults intersect. The core from TG-4 is then well suited to test models of reservoir

evolution as discussed above. The cores consist of interbedded basalt and andesite lavas, andesitic and dacitic tuffs, and mass wasting deposits. Similarities between lithologic units and variable alteration have made traditional stratigraphy unsuccessful. The hydrothermal alteration can take the form of high-density hairline veining, mottled white and green mineralization in the matrix of mass wasting deposits, or pale green mineralization around fracture planes and lithologic contacts that extend several centimeters into the rock. Areas of high permeability are often associated with the brecciated tops of vesicular basalt and andesite flows or with hydrothermally altered and fractured tuffs (Kolker et al., 2011)

3. PALEOMAGNETISM

3.1 Paleomagnetism Methods

The fractured core pieces were reassembled into "runs" using the fit of individual pieces or through-going rock fabric, and a reference mark (N') was made along the length of each section (Figure 2). Each run is separated from the next where the core could not be fitted back together. This disconnect occurs where the core is so heavily fractured as to be rubble, where there are pieces missing, where the core has been cut for sampling without being marked, or where the core pieces were deformed because of drilling complications. Runs that were fully processed were chosen because they contain the highest concentration of cross cutting veins and because they contain the most reliable paleomagnetic directions.

Commonly in paleomagnetic studies a virtual geomagnetic pole (VGP) is calculated from a single paleomagnetic specimen. If VGP's are averaged over ~10,000 years they approximate a geomagnetic axial dipole (GAD) field, which is the first and highest order variable in all paleosecular variation models. As a result, it is considered best practice to sample at least 10,000 years of the rock record to average out this paleosecular variation. Because Akutan is at a high latitude the inclination angle is steep and therefore there is inherent error in the declination direction of any magnetic signal. Also because of the limited usable sample sites, and because the core has not been dated, we assume that there is not enough time sampled to average out paleosecular variation. Paleosecular variation models typically have a virtual geomagnetic pole (VGP) dispersion of about 30° from the GAD field (Johnson and Constable, 1996). Stone and Layer (2006) showed that the paleosecular directions from the Aleutian Islands for 0-2 Ma have a much smaller directional dispersion than what is predicted by current paleosecular variation models. The dispersion measured from flows across the Aleutians have a VGP dispersion of 6.43° from the GAD field, and when data from western Canada is added the VGP dispersion is 12.07°. Therefore, the reoriented structural measurements used in this study have an error of at least ±6.43° and up to ±30° in the strike direction, although the relationship between fracture sets within a single run are accurate and precise.

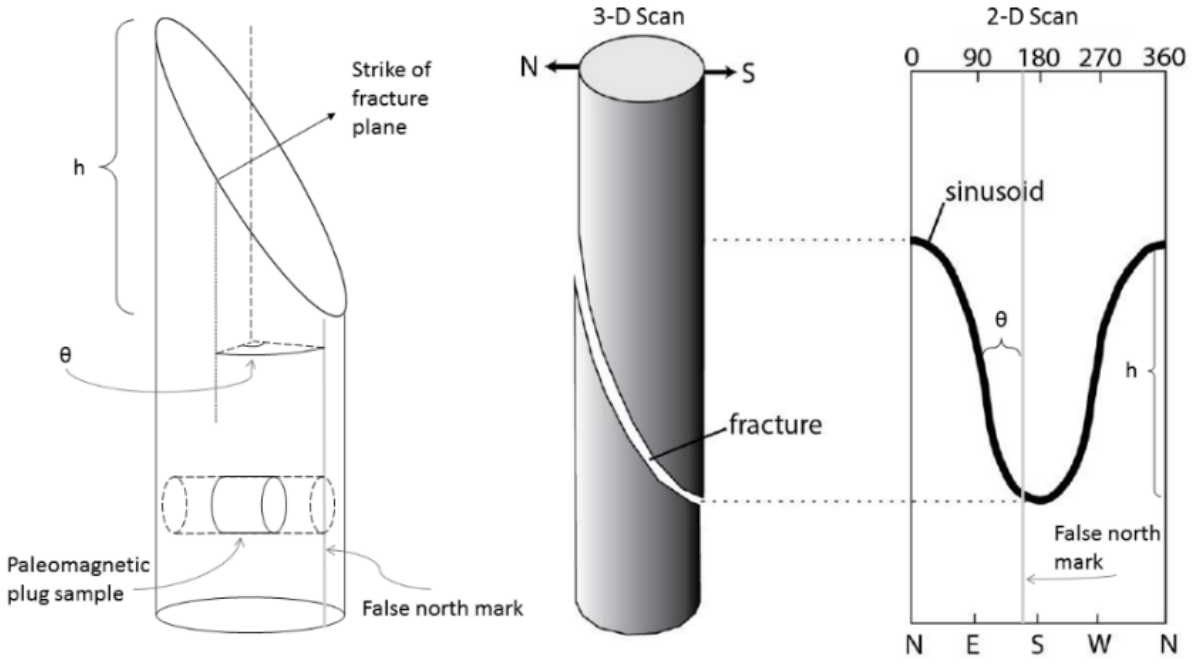

Figure 2: Cartoon showing the position of plug samples for paleomagnetic analysis relative to the false north mark (N'), and a representation of fractures in the 3-D and "unrolled" 2-D states. The height (h) of the sinusoid and the distance from N' to the inflection point (Θ) are used to calculate the strike and dip of the fracture or vein from the 2-D scans.

4. STRUCTURE FROM MOTION

Each selected core run was photographed with a Nikon COOLPIX B500 digital camera. The core segments were placed on a rack with a green screen background, which was masked out of the images. Model building followed the standard Agisoft workflow, and a cylindrical projection was used to create an "unrolled" image of the outside of the core (Figure 2). ImageJ was used to generate a list of pixel coordinates from these images from which the strike, dip, and depth of fractures, veins, contacts and matrix permeability were calculated in an excel spread sheet. The mineral fill was identified, and rake of slicken lines measured by hand. Cross cutting relationships were noted if present. A vein was deemed "cross cutting" where there were subtle offsets or where the mineralization clearly overprinted the other structure. If a fracture or vein was offset by more than a few millimeters it was not measured, as the offset h measurement would not produce and accurate dip data. Instead a mineral of similar orientation within the run was used as a placeholder for the offset structure.

4.2 Core log analysis

A straight fracture in the core appears as a perfect sinusoidal curve in the core log images (Figure 2). To calculate the strike and dip of structures the pixel coordinates of the peak (T) and troughs (B) of the sine curve as well as the coordinates of the N' line, the pixel width of the image, and the pixel lengths of a scale were extracted with the open source software ImageJ and used as inputs in an excel sheet. The vertical scale was used to calculate the depth of each feature at T. The difference between the T and B of the curve (labeled (h) in Figure 2.) is used with the diameter of the core (d) to calculate the dip by

$$dip = tan^{-1}\left(\frac{h}{d}\right) \quad (1)$$

The strike is calculated in the right-hand rule as the inflection point of the curve where the curve increases to the right. The x and y coordinates of the inflection point are calculated as the median value of the x and y coordinates of T and B. The pixel distance between the N' line and the x value of the strike point is the azimuthal strike in the N' coordinate system. The pixel strike is converted to degrees using the conversion factor of

$$\frac{pixel\ width}{360\ deg} \quad (2)$$

The declination of the RM signal chosen for reorientation of the run is then used to convert the strike measurements from the N' coordinate system to true geographic north, albeit with error inherited from the uncertainty of the paleomagnetic directions (see section 3.2.1).

Error is introduced into these calculations as the irregularity of the structural plane increases because the logic of the calculation is based on the perfect sign curve created as the trace of a straight plane. Additionally, if the ball-and-stick model is misshapen significantly the projection will be distorted. It is then important to collect enough overlapping photographs from which to make the models as accurate as possible. A randomly selected subset of orientation data was also measured by hand with a Brunton compass and compared to the calculated orientations. The amount of error on the calculated orientations is comparable to that of measurements made by hand as both are done on a small portion of a much larger plane. Therefore, as with structural measurements made by hand in the field we rely on a large data set to define general orientations of structural features which can be related to island scale trends mapped on the surface.

Any mineral fill present on a fracture or vein was identified and rake of slicken lines were measured by hand. Cross cutting relationships were noted if present. A vein was deemed "cross cutting" if there were subtle offsets or where the mineralization clearly overprinted other structures. If a fracture or vein was offset by more than a few millimeters it was not measured, as the offset h measurement would not produce accurate dip data. Instead, a mineral of similar orientation within the same run was used as a placeholder for the offset structure. This was deemed appropriate as the main goal of noting the cross-cutting relations is to establish age relationships between the three main structural trends mapped at the surface.

4.3 Reoriented structures

The data were first separated into mineralized and un-mineralized structures, i.e. veins and fractures. The orientations of fractures (Figure 3.A) average around horizontal with a random distribution of strikes. These fractures are interpreted to be the result of changing stresses as the core was being drilled and not the result of sustained fluid flow. Structures that are mineralized, i.e. veins, are interpreted to be evidence of fluid flow. Furthermore, veins that have layers of mineralization are interpreted to be evidence of episodic rupture or sustained fluid flow. Veins with a monomineralic fill are more likely the result of a single flow event, however this is not necessarily true. Fractures are not considered further, and all the subsequently discussed veins sets are subsets of the veins presented in Figure 3.B. Mineralized veins have strikes in a wide range of directions however there is a prominent NW striking, NE dipping cluster as well as a more dispersed SE striking, SW dipping cluster.

Vein width, as distinct from aperture which is discussed below, is here defined as the width of the mineralized zone. Although vein widths vary, most are less than 1mm thick (Figure 3.C). Veins that are less than 1mm wide strike predominantly to the NW and dip to the NE, however these narrow veins are observed in nearly all orientations. Veins that are 2-4mm wide are present throughout the bottom three runs and are most abundant in the 313.9 – 324.9 m run. This trend is repeated with veins ranging from 5-9mm wide (Figure 3.E) and veins that are more than 10mm wide (Figure 3.F). Veins of all widths are predominantly striking to the NW and dipping to the NE, with a smaller number of veins striking to the SE and dipping to the SW. Overall the orientation of veins becomes more ordered with depth, with the widest veins present at the greatest depths. Vein width can be interpreted as a large aperture being slowly filled in, indicating high permeability; or a small aperture that is widened over time, indicating sustained fluid flow. As discussed above, laminated veins are evidence of the latter.

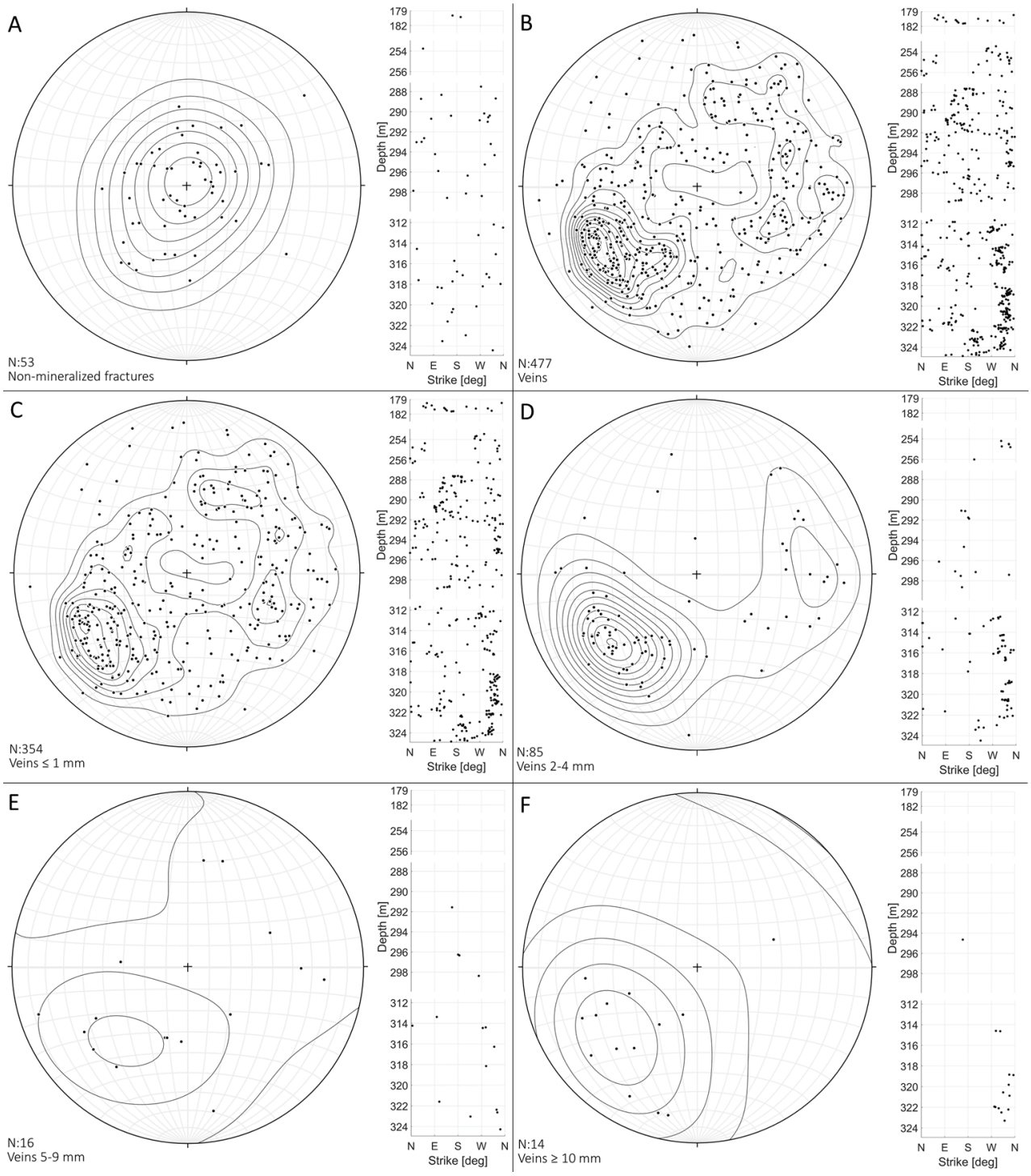

Figure 3. Stereonets of poles to planes for veins that A) have no mineralization on the fracture, B) veins, C) are ≤1mm, D) 2-4mm, E) 5-9mm, and F) >10mm in width. C-F are subsets of the data presented in B. N indicates the number of measurements. Kamb contours have a significance level of 3 and an interval of 2. Note the scale breaks on depth verses strike plots.

4.4 Vein Mineralogy

Calcite filled veins dominate the core (Figure 4.A). Most calcite filled veins are NW striking and dip to the NE, whereas chlorite filled veins (Figure 4.B) are more randomly oriented. Purely chlorite-filled veins are concentrated in the upper portions of the core whereas calcite filled veins are present throughout. Quartz is present in only 13 out of 477 veins and is always accompanied by calcite and or chlorite (Figure 4.C). Veins that have open aperture are concentrated at specific depths (~180 m. depth, between 289-292 m. depth, ~313 m. depth, and ~322 m. depth) rather than a consistent orientation (Figure 4.D). Most apertures are less than 1mm wide however the partially mineralized veins below 322 m depth have apertures up to 2cm wide as well as bladed calcite and argillic alteration and intense veining extending up to 8cm into the wall rock.

4.5 Relative dating of veins

The orientation of veins that are cross-cutting and those that are being cross-cut are very similar. Both conditions have clusters of orientations with strikes to the NW and S with dips to the NE and W respectively. Because of these similarities the fault sets cannot be separated temporally, rather, the data suggest that the fault sets based on orientation are contemporaneous.

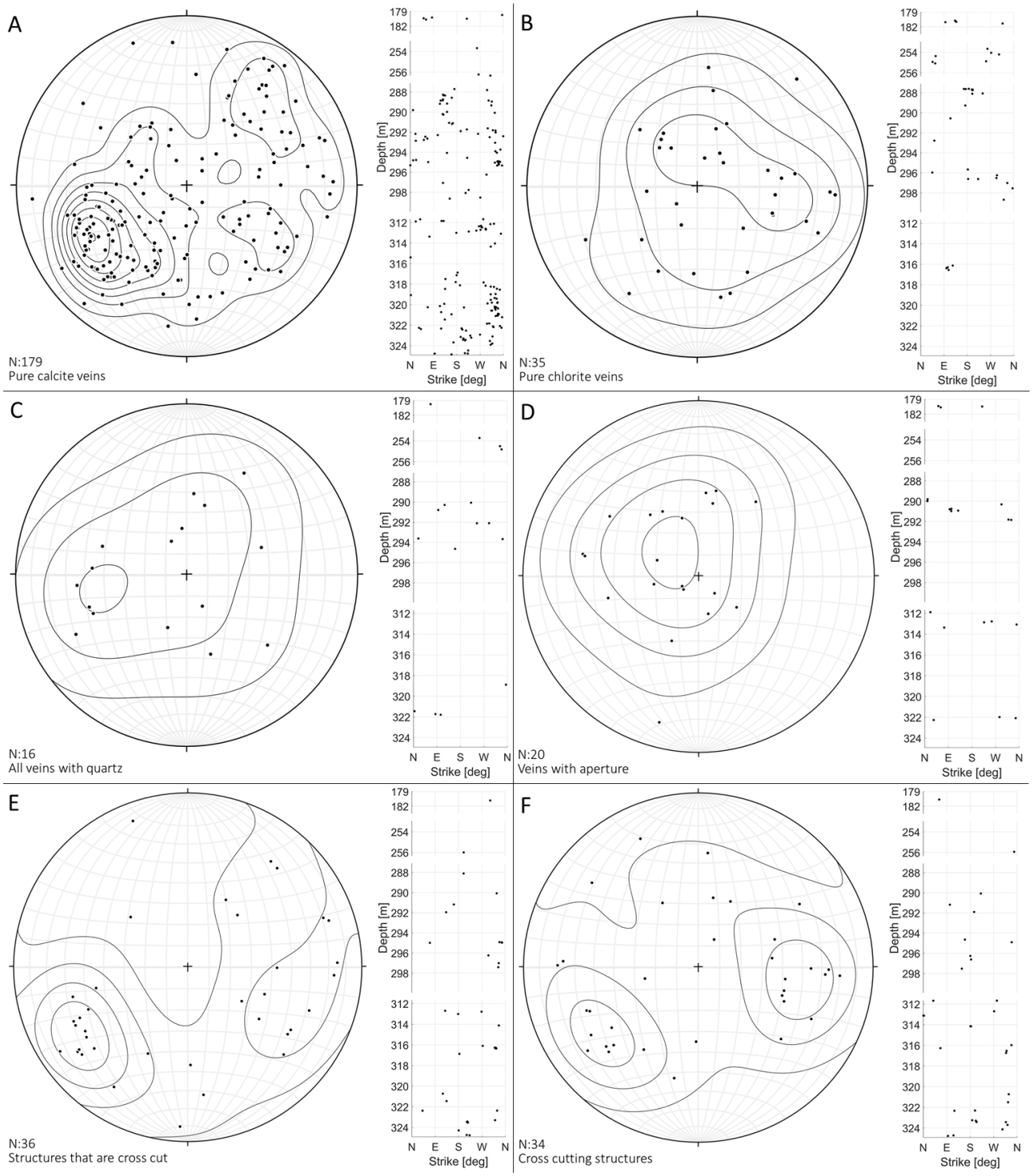

Figure 4. Vein mineralogy. Stereonets of poles to planes for veins that are filled with A) only calcite, B) only chlorite, C) calcite and other minerals, D) chlorite and other minerals, E) quartz and other minerals, and F) partial mineralization with aperture. All data are subsets of the data presented in 6.B. N indicates the number of measurements. Kamb contours have a significance level of 3 and an interval of 2. Note the scale breaks on depth verses strike plots.

5. MULTIPLE INVERSE METHOD

The determination of paleo stresses or in situ stresses from fault slip data has been the goal of many researchers. One of the main failings of many studies is the use of heterogeneous fault slip data for principle stress inversions (Sperner and Zweigel, 2010). Heterogeneous fault slip data is the result of multiple stress states and must be separated into temporal subsets based on geological

evidence or geographical regions of homogenous strain (Simón, 2018). Temporal delimitation is not possible for this study because, as discussed above (section 4.5), cross cutting relations between fault sets based on orientation are inconclusive.

The multiple inverse method (MIM) (Yamaji, 2000) is a statistical algorithm based on the inverse method (Angelier, 1984) that can effectively test whether a set of fault slip data resulted from homogenous or heterogeneous stresses. The MIM calculates a stress tensor which minimizes the angular difference between observed and theoretical slip directions on a set of fault planes. The stress tensor is described by three directional components as well as the Lode number (μ_L) (Lode, 1925) which describes the shape of the stress ellipsoid where,

$$\mu_L = \frac{2\sigma_2 - \sigma_1 - \sigma_3}{\sigma_1 - \sigma_3} \quad (3)$$

given that $\sigma_1 \geq \sigma_2 \geq \sigma_3$. The Lode number ranges from -1 to +1 where the end member values represent compression and tension respectively and intermittent values indicate triaxial strain. While the inverse method uses Bishops parameter (Φ) to describe the shape of a stress ellipsoid the Lode number is more desirable for the MIM algorithm because end members have the same absolute value. The Lode number is related to Φ by $\mu_L = 2\Phi - 1$, and varies from 0 to 1 where the end members compression and tension, respectively. The three directional components and Φ are plotted in a four-dimensional parameter space to define a stress state. The best fit to the input data is indicated by a cluster of similar σ_1 and σ_3 directions with similar Φ values. If multiple clusters (i.e. multiple solutions) are observed the data is said to be heterogeneous; resulting from multiple or changing stress states.

For this study slicken line data was separated based on mineralogy with the reasoning that veins of similar mineralogy formed from a similar fluid source and stress field. Furthermore, veins with a single mineralogy are interpreted to be the result of a single rupturing event while laminated veins have more likely been reactivated by multiple stress fields. Throughout the ~31 m. of reoriented core there are 88 vein or fracture faces with slicken lines. Of these, 58 are high level confidence, and the remaining 30 fracture sets are low level confidence and were not used in the final MIM analysis. Simón (2018) has suggested using at least 10 but preferably 15 faults with directional data in any stress inversion. The MIM program also requires at least 15 data points to produce an interpretable result. Purely calcite filled veins with slicken lines of high confidence numbered 26, while only 10 purely chlorite filled veins with slicken lines of high confidence are present. Veins with chlorite and other minerals, primarily calcite, were added to the chlorite data set to obtain a large enough data set for the MIM to function. Results are presented in Figure 5 and 6.

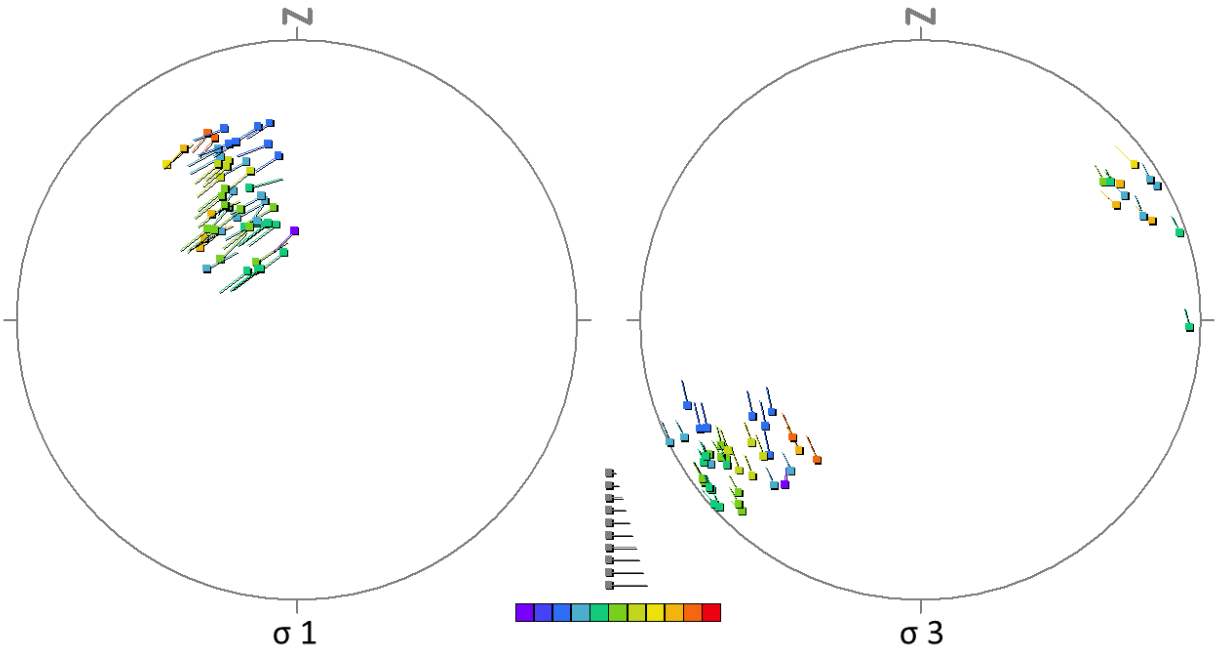

Figure 5. Results of MIM analysis for veins filled with only calcite. Sigma 1 directions are plotted on the left and sigma 3 directions are plotted on the right. Squares indicate directions and the line extending out of each square points in the azimuth direction of the paired direction in the other plot. Longer lines indicate a paired direction with a shallower plunge. Colors indicate the Φ value with purple = 0.1 and red= 1.0. Dispersion factor= 3 and enhancement=15.

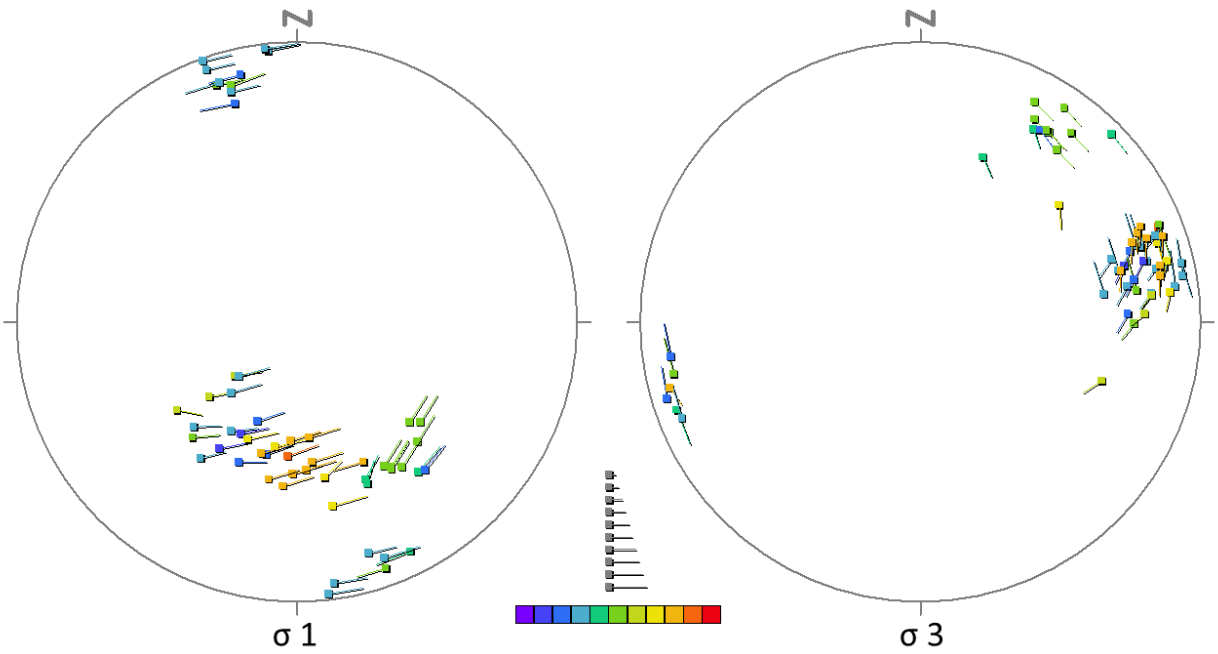

Figure 6. Results of MIM analysis for chlorite ± calcite ± quartz filled veins. Symbology as in Figure 5.

5. DISCUSSION

We have hypothesized that if the 1996 seismic swarm caused an increase in the heat outflow of the hydrothermal system at HSBV by rupturing the NW trending fault, as Bergfeld etal. (2014) suggested, then the NW trending set of veins would be the youngest observed in the core. Cross cutting relations do not support this hypothesis. Rather cross cutting relations (Figure 4.E-F) indicate that the NW and NNE trending fracture sets are conjugate sets and have likely ruptured repeatedly over the lifetime of the hydrothermal system.

The wide, NW trending veins with significant aperture below 314 m as well as the abundance of veins with a NW strike indicate that NW trending structures have been a sustained fluid pathway. The mineralogy of these NW striking veins is predominantly pure calcite, however there are calcite veins with laminations of chlorite and trace amounts of quartz present as well. The pure calcite veins indicate that the NW trending structures act as an inflow pathway. Whereas chlorite and quartz filled veins are indicative of the outflow, as the solubility of calcite decreases with increasing temperature and the solubility of quartz increases with increasing temperature. Because of these inverse solubility trends, hydrothermal calcite is a near ubiquitous sign of fluids moving towards a heat source (the inflow) and quartz is a sign of fluid moving away from a heat source (the outflow). Veins that are laminated with calcite ± chlorite ± quarts could be the result of multiple rupturing events or the result of boiling causing systematic mineralization.

Results of the MIM analysis on purely calcite filled veins show homogenous strain with σ_1 in the NW and σ_3 in the SW (Figure 5.), however Φ values vary from 0 to 0.9 within a single cluster. This varied Φ value could indicate that the intermediate stress varied substantially from very close to σ_1 to very close to σ_3 while the maximum and minimum stresses remained constant. The σ_2 direction corresponding to the data presented in Figure 5 is oriented at approximately 125 degrees, with a plunge of approximately 50 degrees. This orientation of σ_2 (50:125) would be consistent with a variable stress originating from a source SE of and below the TG-4 well cite. As discussed in section 2, the surface deformation of Akutan island before and after the seismic swarm of 1996 has been modeled as the emplacement of a dike under the NW flank of the volcano parallel to NW striking ground cracks observed after the event (Lu et al., 2005). The modeled dike intrusion is NE of the TG-4 well site and prominent ground cracks were observed SE of the TG-4 well site. We propose that this injection and subsequent contraction during cooling could be responsible for the varied Φ values, (i.e. a varied σ_2) observed in the signal from purely calcite filled veins. Additionally, calcite filled veins are prominently NW striking, parallel to the dike intrusion, and represent hydrothermal recharge pathways.

Results of the MIM analysis on chlorite filled veins indicate heterogeneous strain, as there are several clusters of possible solutions (Figure 6). This is not surprising given that the data set contained veins laminated with chlorite +/- calcite. Multiple orientations of slicken lines were observed on two of the veins with laminated mineralogy, where each lamination contained slickenlines of different orientations. These were excluded from the MIM however, multiple orientations of slickenlines is evidence of multiple rupturing events rather than systematic mineralization caused by boiling as discussed above. The two main clusters of solutions with Φ values between 0.2-0.4 ($\sigma_1 \gg \sigma_2 > \sigma_3$) (light and dark blue in Figure 6) have near horizontal σ_3 directions, oriented ENE / WSW. The σ_1 directions vary; one is near horizontal with an azimuth orientation of NNW and the other is near vertical with azimuth orientation in the SW. This combination of high angle and low angle σ_1 values with a consistent σ_3 directions has been interpreted as alternating horizontal compression from tectonic plate movement and vertical compression from overburden pressures. The arc parallel ENE/WSW orientation of σ_3 is consistent with the findings of Lallemant and Oldow (2000), who documented four generations of structural features that are prominent across the curved Aleutian arc. They show that the Aleutian arc is undergoing differential strain accumulation that is manifested as partial block rotation and arc parallel extension.

Stelling et al (2015) has modeled the geothermal reservoir to be directly below the fumaroles at the head of the upper arm of HSBV. Furthermore, Kolker et al. (2012) has proposed two possible outflow paths either to the south and east following the valley floor or

north and east under Mt. Formidable. From this work we can add that the NW trending structures SW of HSBV are likely conducting inflow, while the outflow is defused, utilizing the conjugate NW/NNE fault system that repeatably ruptures because of tectonic stresses. Even though there are three prominent structural orientations mapped on the surface surrounding the TG-4 site, there are only two represented in the cross-cutting relation data. The lack of E-W trending structures indicates that the E-W trending structures might be inactive, at least at the TG-4 locality. The line of hot springs in HSBV (Figure 1) defines a proposed fault (Stelling et al. 2015), however the dip is unconstrained. The southeastern block of the proposed NE trending fault might be an impermeable layer that concentrates the defuse flow, as there are no hot springs to the south of the proposed fault.

6. CONCLUSION

There has been a documented increase in the heat output at the hydrothermal field in Hot Springs Bay valley on Akutan, Alaska. Approximately 31 meters of the TG-4 drill core that was collected in 2010 has been reoriented with the remanent magnetization as an indication of geographic north. Two-dimensional core logs were created from three-dimensional digital reconstructions made with structure from motion software. Veins and structural information were measured from these two-dimensional core logs. This novel application of the software could be used for core log creation, as in this study, or ground truthing down hole geophysical logs.

Results of the multiple inverse method analysis show that Akutan is a structurally dynamic island with tectonic compressional influences causing arc parallel extension, vertical compression from overburden pressure, as well as fluctuating stresses from magmatic intrusions. Stress directions from pure calcite veins are likely a signal from inflation and contraction of the volcano, whereas chlorite and quartz filled veins are produced by heterogeneous strain.

Northwest trending calcite filled veins dominate the core and likely represent a recharge pathway that has rejuvenated the hydrothermal resource and caused the increased outflow documented by Bergfeld et. al. (2014). Cross cutting relational data within the core show a conjugate NW and NNE trending fault system that likely hosts a diffuse outflow. We propose that this diffuse outflow is concentrated along a proposed NE trending fault plane and daylights at the hot springs in the lower valley.

7. ACKNOWLEDGMENTS

This work was funded by the Western Foundation, the Geological Society of America and by the Alaska Geological Society. I would like to thank my committee members for their guidance; Ben Paulsen for his support in creating the drill logs; Russ Burmester, Will Calbert, and Masoud Mirzaei for their support in the at the Northwest Paleomagnetism Lab; Daniel Fagerlie for writing a python script that automated the creation of digital masks; and Nathanial VanArendonk for creating a MATLAB script that made the depth verse strike plots.

REFERENCES

Allerton, S.A., McNeill, A.W., Stokking, L.B., Pariso, J.E., Tartarotti, P., Marton, F.C., and Pertsev, N.N.: Structures and magnetic fabrics from the lower sheeted dike complex of Hole 504B reoriented using stable magnetic remanence, in Proceedings of the Ocean Drilling Program, Scientific Results, 137, (1995), 245–251.

Angelier, J.: Tectonic analysis of fault slip data sets, Journal of Geophysical Research, Solid Earth, 89, (1984), 5835–5848.

Bergfeld, D., Lewicki, J.L., Evans, W.C., Hunt, A.G., Revesz, K., and Huebner, M.: Geochemical investigation of the hydrothermal system on Akutan Islan, Alaska, July 2012, U.S. Geological Survey Scientific Investigations Report Scientific Investigations Report. (2014).

Byers, F.M., and Barth, T.F.W.: Volcanic activity on Akun and Akutan islands, Proceedings Seventh Pacific Sciense Congress, 2, (1953).

Finch, R.H.: Akutan volcano, Volcanological Review, 16, (1935), 155–160.

Hailwood, E.A., and Ding, F.: Palaeomagnetic reorientation of cores and the magnetic fabric of hydrocarbon reservoir sands, Geological Society, London, Special Publications, 98, (1995), 245–258.

Hill, I.A., Taira, A., Firth, J.V.: Proceedings of the Ocean Drilling Program, 131 Scientific Results, Ocean Drilling Program, Proceedings of the Ocean Drilling Program, 131, (1993).

Johnson Catherine L., and Constable Catherine G.: Palaeosecular variation recorded by lava flows over the past five million years: Philosophical Transactions of the Royal Society of London. Series A, Mathematical, Physical and Engineering Sciences, 354, (1996), 89–141.

Kent, D.V., Olsen, P.E., and Witte, W.K.: Late Triassic-earliest Jurassic geomagnetic polarity sequence and paleolatitudes from drill cores in the Newark rift basin, eastern North America, Journal of Geophysical Research, 100, (1995), 14,965-14,998.

Kolker, A., Bailey, A., and Howard, W.: The 2010 Akutan Exploratory Drilling Program: Preliminary Findings, Geothermal Resource Council Transactions, 35, (2011), 847–852.

Kolker, A., Stelling, P., Cumming, W., and Rohrs, D.: Exploration of the Akutan geothermal resource area, in Proceedings, Thirty-Seventh Workshop on Geothermal Reservoir Engineering, 37, (2012).

Lallemant, H.G.A., and Oldow, J.S.: Active displacement partitioning and arc-parallel extension of the Aleutian volcanic arc based on Global Positioning System geodesy and kinematic analysis, Geology, 28, (2000), 739–742.

Lu, Z., Wicks Jr, C., Kwoun, O., Power, J.A., and Dzurisin, D.: Surface deformation associated with the March 1996 earthquake swarm at Akutan Island, Alaska, revealed by C-band ERS and L-band JERS radar interferometry, Canadian Journal of Remote Sensing, 31, (2005), 7–20.

Miller, T.P., McGimsey, R.G., Richter, D.H., Riehle, J.R., Nye, C.J., Yount, M.E., and Dumoulin, J.A.: Catalog of the historically active volcanoes of Alaska, US Geological Survey Open-File Report, 98, (1998), 582.

Motyka, R.J., Liss, S.A., Nye, C.J., and Moorman, M.A.: Geothermal resources of the Aleutian arc, Division of Geological and Geophysical Surveys, (1993).

Motyka, R.J., and Nye, C.J.: A geological, geochemical, and geophysical survey of the geothermal resources at Hot Springs Bay valley, Akutan Island, Alaska, Alaska Division of Geological & Geophysical Surveys Report of Investigations, 115, (1988).

Richter, D.H., Waythomas, C.F., McGimsey, R.G., and Stelling, P.L.: Geology of Akutan Island, Alaska, US Geological Survey Open-File Report, (1998), 98–135.

Romick, J.D., Perfit, M.R., Swanson, S.E., and Shuster, R.D.: Magmatism in the eastern Aleutian arc: temporal characteristic of igneous activity on Akutan Island, Contributions to Mineralogy and Petrology, 104, (1990), 700–721.

Simón, J.L.,: Forty years of paleostress analysis: has it attained maturity? Journal of Structural Geology, (2018).

Sperner, B., and Zweigel, P.: A plea for more caution in fault–slip analysis, Tectonophysics, 482, (2010), 29–41.

Stelling, P., Hinz, N.H., Kolker, A., and Ohren, M.: Exploration of the Hot Springs Bay Valley (HSBV) geothermal resource area, Akutan, Alaska, Geothermics, 57, (2015), 127–144.

Stone, D.B., and Layer, P.W.: Paleosecular variation and GAD studies of 0-2 Ma flow sequences from the Aleutian Islands, Alaska: PALEOSECULAR VARIATION, Geochemistry, Geophysics, Geosystems, 7, (2006).

Yamaji, A.: The multiple inverse method: a new technique to separate stresses from heterogeneous fault-slip data, Journal of Structural Geology, 22, (2000), 441–452.